metals

MDPI

Article

Microstructure and Properties of TiAl-Based Alloys Melted in Graphite Crucible

Wojciech Szkliniarz and Agnieszka Szkliniarz *

Faculty of Materials Engineering, Silesian University of Technology, Krasińskiego 8, 40-019 Katowice, Poland; wojciech.szkliniarz@polsl.pl

* Correspondence: agnieszka.szkliniarz@polsl.pl

Abstract: This paper presents the chemical and phase composition, microstructure, and selected properties both at room temperature and at the temperature corresponding to the expected operating conditions of three successive generations of TiAl-based alloys (Ti-47Al-2W-0.5Si, Ti-45Al-8Nb-0.5(B,C), and Ti-45Al-5Nb-2Cr-1Mo-0.5(B,C)-0.2Si) melted in a vacuum induction furnace with high-density isostatic pressed graphite crucibles. The obtained results of mechanical and physical properties of the produced alloys were compared to the properties of reference alloys with similar chemical composition and melted in a cold copper crucible furnace. The effect of increased carbon content in the produced alloys due to the degradation of the graphite crucible during melting is higher strength properties, lower plastic properties, higher coefficient of thermal expansion, and improved creep resistance. It was shown that the proposed technology could be successfully used in the production of different generation TiAl-based intermetallic alloys.

Keywords: TiAl-based alloys; induction melting; graphite crucibles; microstructure; mechanical properties

Citation: Szkliniarz, W.; Szkliniarz, A. Microstructure and Properties of TiAl-Based Alloys Melted in Graphite Crucible. *Metals* **2021**, *11*, 669. https://doi.org/10.3390/met11040669

Academic Editor: Martin Heilmaier

Received: 15 March 2021
Accepted: 15 April 2021
Published: 20 April 2021

1. Introduction

TiAl intermetallic alloys with high melting point, low density, high specific strength and stiffness, and good creep and oxidation resistance are an exceptionally attractive and lightweight new generation construction material suited for use for aircraft and car engine components, spacecraft construction and sheathing, and gas turbines used in the power generation sector in the temperature range of 600 to 850 °C [1–5]. The highest expectations concern their use as substitutes for expensive nickel superalloys with twofold greater density in the production of rotating construction components of advanced aircraft engines such as low-pressure turbine blades and high-pressure compressor rotor blades. The use of such substitutes is expected to improve the performance of engines, increase their energy efficiency, and reduce exhaust gas emissions [2,5].

Although new powder-based technologies for manufacturing complex components such as additive manufacturing [6] and spark plasma sintering [7] are becoming increasingly more interesting for the production of very complex γ-TiAl-based components, melting and casting nowadays still represent one of the most useful methods for the production of TiAl-based alloys. Basically, melting technologies used in the titanium industry such as vacuum arc remelting, plasma arc melting, and electron beam cold hearth melting are applicable to TiAl alloys as well [8]. Currently, almost all titanium alloys are melted and cast by vacuum arc remelting or induction skull melting using rammed graphite molds for casting [9].

The use of conventional induction melting, with a ceramic, refractory metal, or graphite crucible, as an alternative method of production, can bring many benefits like lower melting and investment costs, easier operation procedures, and higher superheating [10]. This is also a promising method for medium-to-large scale production of castings,

allowing for quality castings to be obtained by homogeneous stirring and applicable superheat of the melt. However, for titanium alloys, the main problem is the very high reactivity of these alloys in a liquid state by contact with gases and ceramic materials as well as low castability and high casting contraction. The aggressive crucible–melt interaction is a result of this reactivity and causes melt contamination, alloy heterogeneity, non-metallic-inclusions, and premature crucible failure [9–11]. This makes it extremely difficult to design an effective and inexpensive crucible material, and until now a material for the crucible that is completely inert against titanium and its alloys has not been found. It is still a challenge.

Among many investigated various refractory materials, only several can be successfully used for melting and casting of TiAl alloys, such as Y_2O_3, ZrO_2, CaO, Al_2O_3, ThO_2, $BaZrO_3$, $CaZrO_3$, BN, AlN, and graphite [9–11]. Each of these refractories has drawbacks and more or less cause the ingot contamination by crucible material. Furthermore, the use of Y_2O_3 and ZrO_2 is limited by their high cost; Al_2O_3 by low melting temperature; ThO_2 by radioactivity; and CaO by its high humidity, poor thermal shock resistance, and associated instability.

Graphite is attractive because it has appropriate electrical properties, good formability, good resistance for thermal cracking, high melting temperature, and is relatively cheap.

A few researchers presented results of induction melting of titanium aluminides in a graphite crucible and each confirmed the increased content of carbon in ingot. Barbosa assessed that graphite crucible used in induction melting of Ti-48Al is absolutely useless due to the high carbon content in the casting (up to 7.0%) [12]. Čegan et al. [13] connected the value of carbon content in the investigated alloys (Ti-47Al and Ti-47Al-0.3Y) melted in an extruded graphite crucible with the melt stabilization time. In their further work, Čegan et al. [14] recognized that induction melting of Ti-47Al-(8Nb or 8Ta-0.3Y) in graphite crucible and centrifugal casting into graphite mold could be considered a suitable method for preparation of TiAl-based alloys, despite the increase in carbon content from 460 to 1020 wt. ppm resulting in the formation of fine carbide particles. The authors based the study of mechanical properties on compression tests. Kamyshnykova and Lapin [8,15] stated that induction melting of intermetallic alloy in graphite crucibles and centrifugal casting into cold graphite mold increased carbon content and affected the solidification path.

On the other hand, it is well known that carbon improves the mechanical properties of TiAl-based alloys such as hardness, strength, as well as high-temperature strength and creep resistance [16–18].

The authors' previous experience in the selection of parameters of titanium alloy melting in graphite crucibles shows that in order to obtain a good quality alloy, it is necessary to minimize the aggressive effect of liquid alloy on the crucible's graphite material by reducing the temperature and melting time to the level required to melt the charge and dissolve the alloying components, conduct the melting process under the argon shield, and use the charge consisting of technically pure titanium and master alloy, which is an aluminum alloy with other alloying components rather than pure components. It allows for production of alloys with an assumed and reproducible chemical composition and minimum content of gaseous pollutants [19–22].

The aim of this work is to present complex characteristics of three TiAl-based alloys (representing different generations of these alloys) made by induction melting in a special graphite crucible and compare the chemical composition, microstructure, and some mechanical and physical properties of produced alloys with counterparts made by ceramic crucible-free methods.

2. Materials and Methods

The investigations described in the paper concerned the produced alloys Ti-47Al-2W-0.5Si, Ti-45Al-8Nb-0.5(B,C) and Ti-45Al-5Nb-2Cr-1Mo-0.5(B,C)-0.2Si and the corresponding reference alloys ABB-2, TNB-V2, and TNM-B1, respectively, with chemical compositions

as shown in Table 1, representing respectively the second, third, and fourth generation of TiAl intermetallic alloys.

Table 1. Chemical composition of produced and reference alloys.

Alloy	Chemical Composition											
	Al	W	Nb	Cr	Mo	Si	C	B	Ti	O	N	H
	at.%									ppm		
Ti-47Al-2W-0.5Si	46.60	2.33	-	-	-	0.43	0.35	-	Balance	836	120	21
ABB-2	47.10	2.10	-	-	-	0.50	0.21	-		820	135	24
Ti-45Al-8Nb-0.5(B,C)	44.25	-	7.34	-	-	-	0.34	0.15		935	96	17
TNB-V2	45.40	-	8.10	-	-	-	0.20	0.20		800	100	30
Ti-45Al-5Nb-2Cr-1Mo-0.5(B,C)-0.2Si	43.94	-	4.71	1.77	0.90	0.21	0.34	0.14		939	105	18
TNM-B1	43.50	-	4.00	-	1.00	-	0.10	0.10		900	100	20

The procedure for producing and preparing alloys for tests consisted of the following steps:

— Melting, according to the procedure described in detail in [21–23], carried out in an induction vacuum furnace with a special crucible of 2.0 L made of high-density isostatic pressed graphite (Figure 1), using a charge consisting of technically pure titanium (Grade 2); master alloys (at.%) Al-4W-1Si, Al-16Nb, and Al-10Nb-4Cr-2Mo-0.4Si for Ti-47Al-2W-0.5Si, Ti-45Al-8Nb-0.5(B,C), and (Ti-45Al-5Nb-2Cr-1Mo-0.5(B,C)-0.2Si, respectively; glassy carbon; and crystalline boron.
— Casting into graphite molds in the form of ingots of 55 mm in diameter and 400 mm in length (Figure 1),
— Homogenizing by isothermal soaking at 1400 °C (Ti-47Al-2W-0.5Si) or 1350 °C (remaining alloys) for 1 h combined with furnace cooling after soaking,
— Argon-shielded hot isostatic pressing at 1260 °C and 170 MPa for 4 h.

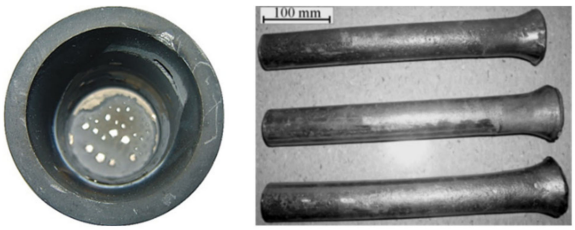

Figure 1. Graphite crucible and manufactured ingots of Ti-47Al-2W-0.5Si alloy.

The program included the investigations of the chemical composition, microstructure, and major properties of the alloys relevant to their expected operating conditions. The temperatures at the end of the most important phase transition $\alpha + \gamma \rightarrow \alpha$, thermal expansion coefficients, strength and plastic properties, modulus of longitudinal elasticity at room temperature and up to 1000 °C, and creep strength at a temperature close to the operating temperature were determined, respectively. When assessing the suitability of the proposed melting technology, the microstructure and physical, chemical, mechanical, and operating properties of the manufactured alloys were compared to the microstructure and properties of the corresponding reference alloys with similar chemical compositions, but melted in cold copper crucible furnaces, and then homogenized and hot isostatic pressed under the same conditions as the manufactured alloys. The chemical composition of the ABB-2, TNB-V2, and TNM-B1 reference alloys is shown in Table 1. The purpose of the comparison

was to provide a positive or negative recommendation for the proposed melting technology as a significantly cheaper alternative to these and other TiAl-based alloys.

The samples for microstructural investigations were prepared using the standard procedure and etched with Kroll reagent. The examinations of microstructure were carried out with Nikon Epiphot 200 optical microscope. The phase composition of the alloy was identified with JEOL JDX-7S X-ray diffractometer. The transformation temperature and linear thermal expansion coefficients were determined with DIL805 dilatometer by Bähr Thermoanalyse GmbH equipped with the LVDT measuring head and the computer control and recording system for experimental data. The tests were carried out on special samples of 4 mm in diameter and 10 mm in length with a 2 mm hole. The measurements were made under vacuum. The induction heating of the samples was carried out at a rate of 3 °C/min. After reaching the desired temperature, the samples were cooled to room temperature at the same rate. As a result of the investigations, the values of average coefficient of linear expansion, thermal expansion coefficient, and characteristic phase transition temperatures during heating and cooling were determined. The investigations of mechanical properties (strength and plastic properties and modulus of elasticity) were based on the static tensile test conducted at room temperature and in the temperature range of up 1000 °C using Z100 Zwick/Roell machine. The creep tests were carried out with creep-testing machines by Applied Test Systems Inc. under standard conditions for this group of alloys—temperature: 760 °C; stress: 207 MPa. Comparative creep tests were conducted on cylindrical specimens with a gauge length of 25 mm (100 mm total length) and gauge diameter of 6 mm according to the ASTM E 139 procedure. The specimens were placed in the furnace under a preload not exceeding 10% of the working load and held at this load while reaching the test temperature. The test temperatures were maintained constant with a precision of ±1.5 °C and monitored for 1 h before the test. The temperature was monitored with two thermocouples touching the specimen gauge section. The elongation of the loaded specimen was recorded at 12 s intervals for the first 10 min of the test and at 4 min intervals for the remainder of the test. The creep test was stopped after 200 h.

3. Results

3.1. Chemical Composition

The average chemical composition of both the produced and reference alloys is shown in Table 1. The obtained Ti-47Al-2W-0.5Si, Ti-45Al-8Nb-0.5 (B,C), and Ti-45Al-5Nb-2Cr-1Mo-0.5(B,C)-0.2Si alloys have very high purity. The content of none of the gaseous impurities (oxygen, nitrogen and hydrogen) exceeds the strict level that characterizes alloys melted in cold crucible furnaces (Table 1). However, during induction melting in a graphite crucible, ~0.1 wt.% (which corresponds to 0.34 at.%) of carbon is passed into liquid alloy due to a partial degradation of the crucible. The carbon content in the obtained alloys is significantly lower than that in the Ti-48Al alloys inductively melted by Barbosa et al. [10,24] and by Klimová et al. [16] in graphite crucibles and comparable to the contents determined for Ti-47Al-8Nb and Ti-47Al-8Ta alloys inductively melted by Čegan et al. [13,25] in crucibles also made of isostatic pressed graphite. This is caused by some alloying additions, like Nb or Ta, which significantly increase the solubility limit of C within the γ-phase due to the formation of antisite defects leading to a certain content of beneficial Ti6-type octahedral sites [26–28]. For binary γ-TiAl based alloys, C-solubility in the γ-phase (L10-structure) is very low.

Carbon is an interstitial element that occurs in TiAl alloys and forms the secondary solid solutions based on the α_2-Ti_3Al and γ-TiAl intermetallic phases, which are present in these alloys, and the carbides if the carbon content exceeds the maximum solubility in the α_2 and γ phases [26]. The solubility of carbon in the α_2 phase is two or three times higher than that in the γ phase. This is because the interstitial elements (oxygen, nitrogen, hydrogen, carbon, and boron) prefer octahedral positions surrounded by six Ti atoms, which occur in the D019 structure of the α_2 phase, but are not present in the γ phase [27,29].

Previous studies have shown that carbon added to TiAl intermetallic alloys with contents not exceeding 0.5 at.% significantly improves their mechanical properties at room and elevated temperature and creep resistance [16,18,25–28,30–32], while carbon added with higher contents less than 1.0 at.% becomes an effective modifier [33]. The improvement in the mechanical properties of carbon-containing TiAl intermetallic alloys is a result of the solid solution hardening due to the penetration of carbon into the structure of secondary solid solutions based on the α_2 and γ intermetallic phases and of the precipitation hardening, due to the presence of dispersive precipitates of Ti_2AlC or Ti_3AlC carbides [14,18,27,28,31,32]. When occurring at the grain boundaries, at the intercrystalline boundaries of the α_2 and γ phase lamellar precipitates, and in the γ phase matrix, these carbides result in grain refinement, reduced interlamellar spacing in alternating colonies of the α_2 and γ phases, and block dislocation movement, thus contributing to the increase in hardening [18,29,31,32,34].

The positive effect of carbon on the mechanical properties and creep resistance of TiAl intermetallic alloys does not depend on whether carbon is added intentionally or penetrates into liquid alloys during the melting process. Therefore, carbon penetration into liquid alloys melted in a graphite crucible due to a crucible degradation caused by the effects of highly reactive liquid titanium should not be a problem unless the carbon content in the obtained alloys exceeds 0.5 at.%. Carbon penetration into liquid alloys should not be a problem either for alloys which, by nature, contain carbon in their chemical compositions, as the knowledge of the scale of the penetration and the target carbon content in alloy makes it possible to adjust the content at the stage of charge preparation for melting.

3.2. Microstructure

The microstructure of the obtained alloys after homogenizing and hot isostatic pressing consists of the γ and α_2 intermetallic phases and the ordered β(B2) phase (Figures 2–4). The presence of the latter was confirmed by X-ray phase analysis for the Ti-45Al-5Nb-2Cr-1Mo-0.5(B,C)-0.2Si alloy only, which contains Nb, Cr, and, above all, Mo—the stabilizing elements of this phase (Figure 3). Different levels of Al and other elements in the obtained alloys result in a significant variation in the morphology of their microstructural components.

The microstructure of the Ti-47Al-2W-0.5Si alloy containing high-melting W after homogenizing and hot isostatic pressing shows the morphological features characteristic of the lamellar microstructure. The alternating colonies of lamellar precipitates of the α_2 and γ phases are present within the large-size grains of the primary α phase (Figure 2). The Al-rich γ phase occurs at the primary grain boundaries, and fine W-rich precipitates of the probably ordered β(B2) phase are present within this phase [19,23].

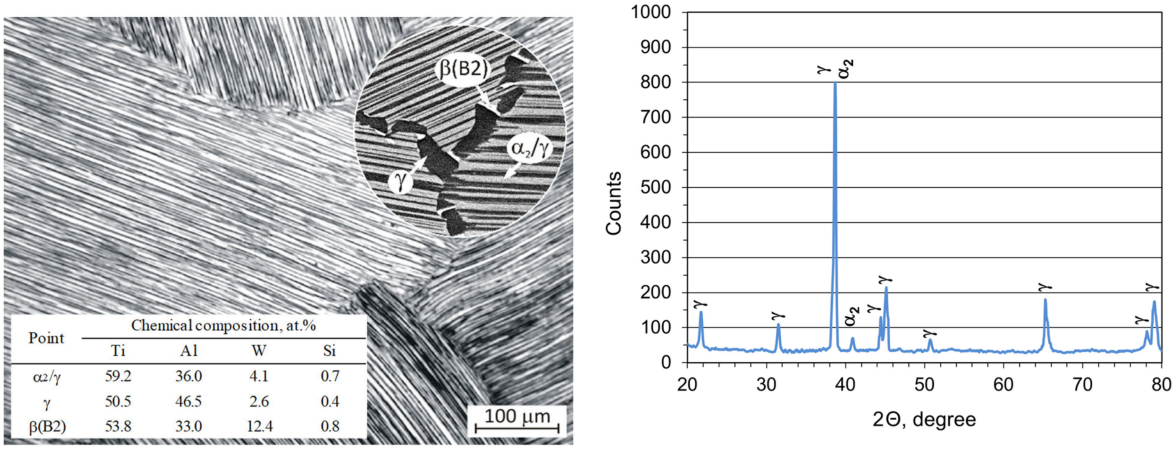

Point	Chemical composition, at.%			
	Ti	Al	W	Si
α2/γ	59.2	36.0	4.1	0.7
γ	50.5	46.5	2.6	0.4
β(B2)	53.8	33.0	12.4	0.8

Figure 2. Microstructure and X-ray diffraction patterns of Ti-47Al-2W-0.5Si alloy.

On the other hand, the microstructure of the Ti-45Al-8Nb-0.5(B,C) alloy with high Nb content after homogenizing and hot isostatic pressing shows the morphological features characteristic of the pseudo-lamellar microstructure which consists of the colonies of alternating thick-lamellar precipitates of the α_2 and γ phases and the uniaxial grains of the Al-rich γ phase occurring at the boundaries of these colonies (Figure 3). Within the γ phase grains, there are Nb-rich precipitates of the probably ordered β phase (B2).

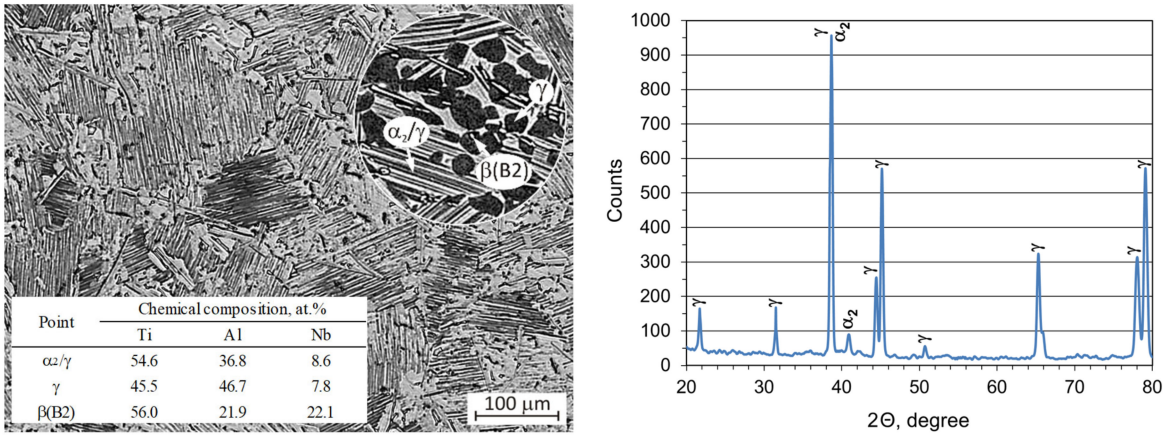

Point	Chemical composition, at.%		
	Ti	Al	Nb
α2/γ	54.6	36.8	8.6
γ	45.5	46.7	7.8
β(B2)	56.0	21.9	22.1

Figure 3. Microstructure and X-ray diffraction patterns of Ti-45Al-8Nb-0.5(B,C) alloy.

The microstructure of the Ti-45Al-5Nb-2Cr-1Mo-0.5(B,C)-0.2Si alloy with a complex chemical composition and containing the β-phase stabilizing elements after homogenizing and hot isostatic pressing shows the morphological features characteristic of the duplex microstructure with the lamellar and uniaxial constituent (Figure 4). It consists of the colonies of fine-lamellar α_2- and γ-phase precipitates with a high degree of refinement, especially in the areas close to the grain boundaries, surrounded by the Al-rich γ phase grains within which the Nb-, Cr-, and Mo-rich precipitates of the ordered β(B2) phase of varying sizes occur. Due to the large proportion of the ordered β(B2) phase in the microstructure of this alloy as compared to the two other alloys, the presence of reflections from this phase were found on the X-ray pattern (Figure 4).

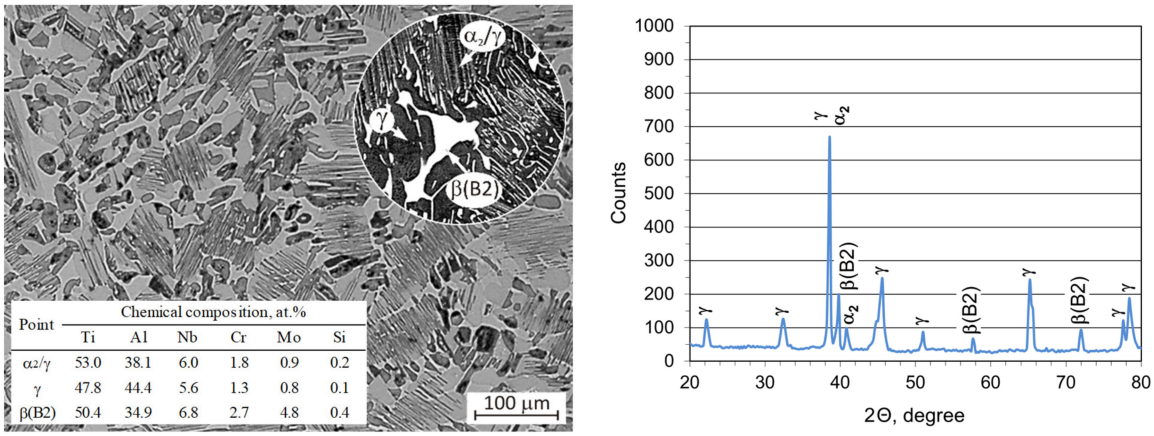

Point	Chemical composition, at.%					
	Ti	Al	Nb	Cr	Mo	Si
α2/γ	53.0	38.1	6.0	1.8	0.9	0.2
γ	47.8	44.4	5.6	1.3	0.8	0.1
β(B2)	50.4	34.9	6.8	2.7	4.8	0.4

Figure 4. Microstructure and X-ray diffraction patterns of Ti-45Al-5Nb-2Cr-1Mo-0.5(B,C)-0.2Si alloy.

The examinations of the microstructure using the transmission electron microscope and the electron diffraction method showed the presence of the following primary phases in the microstructure of the manufactured alloys, in addition to the three ones identified with X-ray examinations: γ, α_2, and β(B2) (Figures 2–4), dispersive precipitates of Ti_5Si_3 silicides (Figure 5a) in the silicon-containing alloys, TiB or Ti_2B_5 borides (Figure 5b) in the

boron-containing alloys, Ti_2AlC carbides (Figure 6a) in the Ti-47Al-2W-0.5Si and Ti-45Al-5Nb-2Cr-1Mo-0.5(B,C)-0.2Si alloys, and Ti_3AlC carbides (Figure 6b) in the Ti-45Al-8Nb-0.5(B,C) alloy.

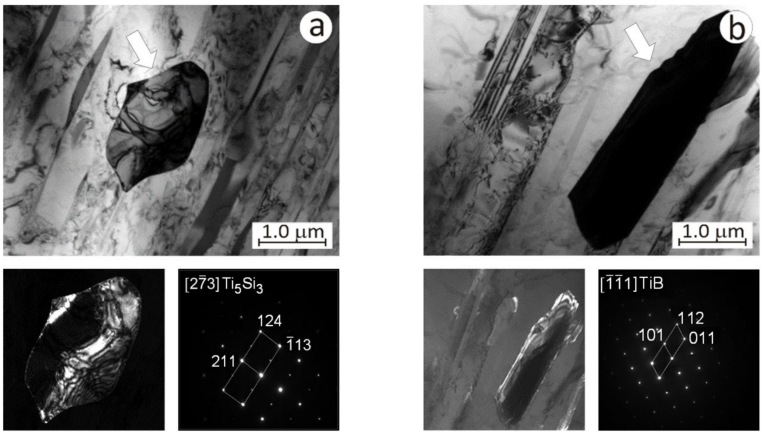

Figure 5. Microstructure and diffraction pattern of silicide (**a**)and boride (**b**) precipitate in Ti-47Al-2W-0.5Si and Ti-45Al-5Nb-2Cr-1Mo-0.5(B,C)-0.2Si alloys, respectively.

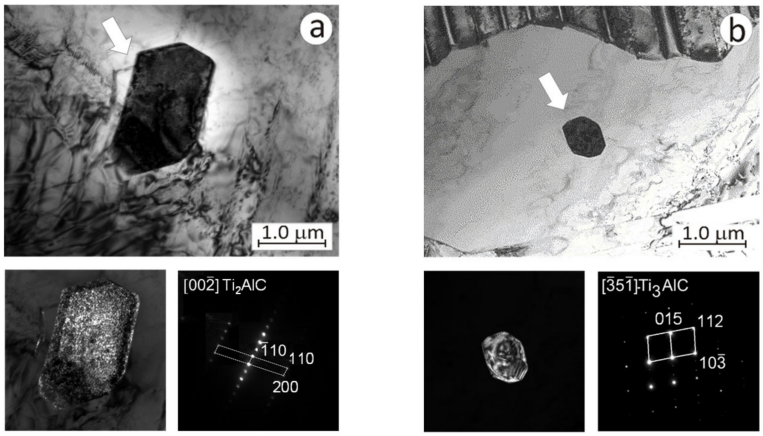

Figure 6. Microstructure and diffraction pattern of carbide precipitate in Ti-45Al-5Nb-2Cr-1Mo-0.5(B,C)-0.2Si (**a**) and Ti-45Al-8Nb-0.5(B,C) (**b**) alloys.

The different types of carbides present in the manufactured alloys containing almost identical carbon content of ~0.35 at.% and the difficulties in revealing them in the microstructure of alloys are justified by the results of the previous studies including, but not limited to, those by Gerling et al. [34] and Stark et al. [26]. Gerling et al. [34] did not find the presence of carbides in the microstructure of the Ti-45Al-5Nb alloy containing even up to 0.5 at.% of carbon and related that fact to the likely increase in solubility of carbon in the α_2 and γ phases due to the presence of dissolved Nb in these phases. They also expressed a hypothesis that a higher carbon content was required to form carbides in TNB alloys. The hypothesis was confirmed by the studies by Stark et al. [26], who demonstrated that the maximum solubility of carbon in the Ti-45Al-5Nb alloy was 0.75 at.% and Ti_2AlC carbides occurred in the alloy only after the indicated carbon content was exceeded.

The positive effect of Nb on the increase in solubility of carbon in the α_2 and γ phases present in TiAl intermetallic alloys [26,35] allows a higher solubility of carbon to be expected in the produced Ti-45Al-8Nb-0.5(B,C) alloy with a higher Nb content compared to the Ti-45Al-5Nb-2Cr-1Mo-0.5(B,C)-0.2Si alloy with a lower Nb content. It is likely for the same reason that Ti_3AlC carbides poorer in carbon are present in the Ti-45Al-8Nb-0.5(B,C) alloy with a higher Nb content, whereas Ti_2AlC carbides richer in carbon are observed in the Ti-

45Al-5Nb-2Cr-1Mo-0.5(B,C)-0.2Si alloy with a lower Nb content and the Ti-47Al-2W-0.5Si, which does not contain Nb.

In turn, the occurrence of carbides in the produced alloys with carbon content of ~0.35 at.% (Figure 6) should be associated with the presence of boron [18,36,37] which, as an interstitial element like carbon, effectively reduces the solubility of carbon in the α_2 and γ phases. For this reason, the carbon and boron content in TiAl alloys is usually considered jointly.

It appears from the example comparison of microstructures of the produced Ti-45Al-8Nb-0.5(B,C) alloy and the TNB-V2 reference alloy, both after homogenizing and hot isostatic pressing under the same conditions, as shown in Figure 7, that the two alloys show the morphological features characteristic of the pseudo-lamellar microstructure and the close similarity to each other within the limits defined by the content of aluminum which, as the main component of alloys, determines the share of the primary α_2 and γ phases in the microstructure.

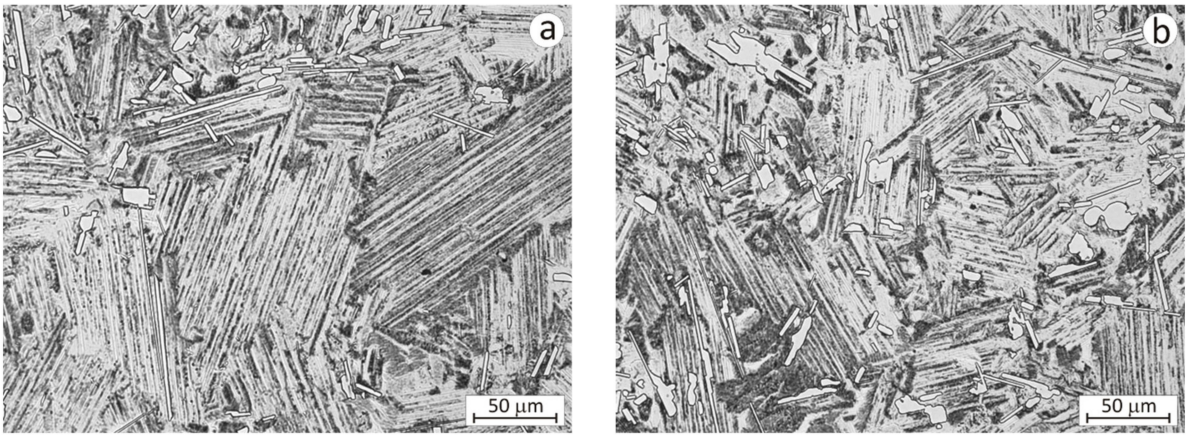

Figure 7. Microstructure of produced Ti-45Al-8Nb-0.5(B,C) (**a**) and reference TNB-V2 (**b**) alloys.

3.3. Physical Properties

Table 2 shows the results of dilatometric measurements in the form of the temperature at the end of the $\alpha + \gamma \rightarrow \alpha$ phase transition, which occurs while heating the produced and reference alloys. This temperature is required to determine the temperature of the major technological processes, e.g., plastic treatment and heat treatment. Data in Table 2 show that this temperature is high and its variation between the manufactured alloys and the reference alloys is approximately ± 10 °C. These small deviations are the result of a slight variation in the chemical compositions of the manufactured and reference alloys (Table 1), given the positive effects of the aluminum content and the negative ones of the niobium content on the temperature values at the end of the $\alpha + \gamma \rightarrow \alpha$ phase transition [28,32,35].

Table 2. Phase transition end temperatures $\alpha + \gamma \rightarrow \alpha$ of produced and reference alloys.

Alloy	Temperature, °C
Ti-47Al-2W-0.5Si	1360
ABB-2	1370
Ti-45Al-8Nb-0.5(B,C)	1318
TNB-V2	1330
Ti-45Al-5Nb-2Cr-1Mo-0.5(B,C)-0.2Si	1310
TNM-B1	1298

The mean values of the linear thermal expansion coefficients determined for the examined alloys based on dilatometry are slightly higher for the produced alloys compared

to the corresponding values for the reference alloys (Table 3), and they are much lower compared to the currently used nickel superalloys (12.8–16.0) and close to titanium alloys (8.6–10.8) [1,38].

Table 3. Thermal expansion coefficient of produced and reference alloys, $10^{-6}/°C$.

Alloy	Temperature Range, °C									
	20–100	**20–200**	**20–300**	**20–400**	**20–500**	**20–600**	**20–700**	**20–800**	**20–900**	**20–1000**
Ti-47Al-2W-0.5Si	10.05	10.41	10.80	11.04	11.30	11.57	11.84	12.19	12.58	13.00
ABB-2	10.00	10.31	10.70	10.92	11.12	11.35	11.66	11.96	12.45	12.89
Ti-45Al-8Nb-0.5(B,C)	10.39	10.61	10.84	11.06	11.22	11.44	11.6	11.8	11.99	12.24
TNB-V2	10.26	10.45	10.66	10.88	11.06	11.29	11.48	11.68	11.93	12.19
Ti-45Al-5Nb-2Cr-1Mo-0.5(B,C)-0.2Si	10.67	10.89	11.10	11.27	11.35	11.39	11.56	11.73	11.98	12.22
TNM-B1	10.09	10.36	10.64	10.81	11.08	11.19	11.31	11.60	11.89	12.19

As shown in the case of the Ti-45Al-8Nb-0.5(B,C) and TNB-V2 alloys (Figure 8), and also in Table 3 for the remaining ones, the changes in values of the linear thermal expansion coefficients are linear between the room temperature and 1000 °C. The similarity of the linear thermal expansion coefficients of these alloys, with regard to the value and linear nature of changes in the entire temperature range of their potential application with titanium alloys and nickel superalloys, is extremely important under the conditions of their coexistence. The lower value of the linear thermal expansion coefficients of the TiAl-based alloys compared to nickel superalloys guarantees greater dimensional stability of the elements made of them, e.g., valves and blades [39].

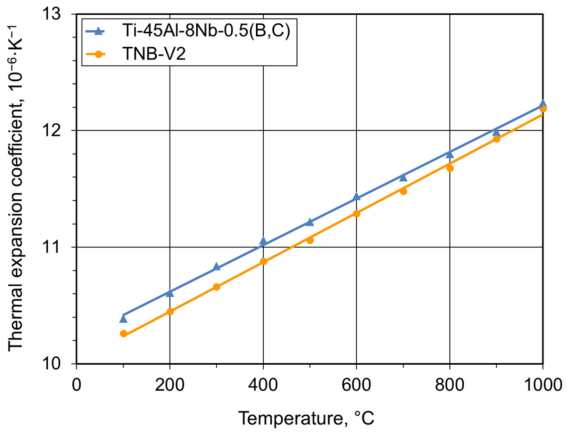

Figure 8. Linear thermal expansion coefficient of Ti-45Al-8Nb-0.5(B,C) and TNB-V2 alloys.

As the temperature increases, the difference between the values of the linear thermal expansion coefficients of the produced and reference alloys becomes increasingly lower (Figure 8; Table 3), which, given the relationship found between the values of the linear thermal expansion coefficients and the phase composition of the alloys [38], may suggest a greater similarity of the phase composition of the produced and reference alloys.

Note that linear thermal expansion coefficients are a function of the thermal and elastic properties of the individual components as well as the atomic structure of the final composition. Lower thermal expansion offers a potential advantage in efficiency by reducing leakage at seals and other structures that control clearances. In addition, note that lower linear thermal expansion coefficients reduce thermal stresses and increase thermal shock and fatigue resistance.

3.4. Mechanical Properties

Figure 9 shows the stress versus strain representative curves of the Ti-45Al-8Nb-0.5(B,C) alloy obtained at room and elevated temperatures by means of static tensile test. The stretching of the alloy under static tensile test conditions is accompanied by plastic strain. At room temperature, its value only exceeds the level of 0.2%, necessary to determine the value of the yield strength, and amounts to ~1.0%. With the temperature increase, plastic strain significantly increases to the value of 4.5 and 9.3% at temperatures of 750 and 950 °C, respectively. This is done at the cost of a reduction in strength, which is especially high at 950 °C.

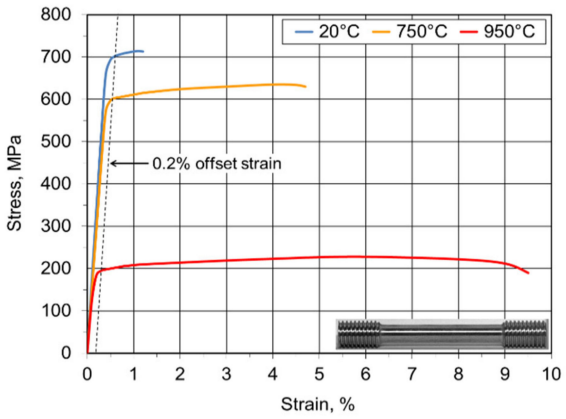

Figure 9. Stress vs. strain representative curves of the Ti-45Al-8Nb-0.5(B,C) alloy obtained at room and elevated temperatures by means of static tensile test.

Figure 10 compares the strength properties (tensile strength and proof stress), modulus of longitudinal elasticity, and plastic properties (elongation) of the produced and reference alloys at room and elevated temperatures (750 and 950 °C), which determine, respectively, the minimum and, after the application of protective coatings [40], the maximum operating temperature for these alloys. These data show that the tensile strength and the proof stress as well as the modulus of longitudinal elasticity of the produced alloys are significantly higher, while the elongation is much lower compared to the properties of the reference alloys. Although relatively slight at room temperature, these differences deepen at 750 and 950 °C. It was found that the strength properties and the modulus of longitudinal elasticity decreased, while the plastic properties increased, with the increase in test temperature. These changes were slight at 750 °C and much higher at 950 °C. The changes in properties with the increase in temperature apply equally to both the produced and reference alloys, without affecting the beneficial relationships produced among different groups of properties (Figure 10).

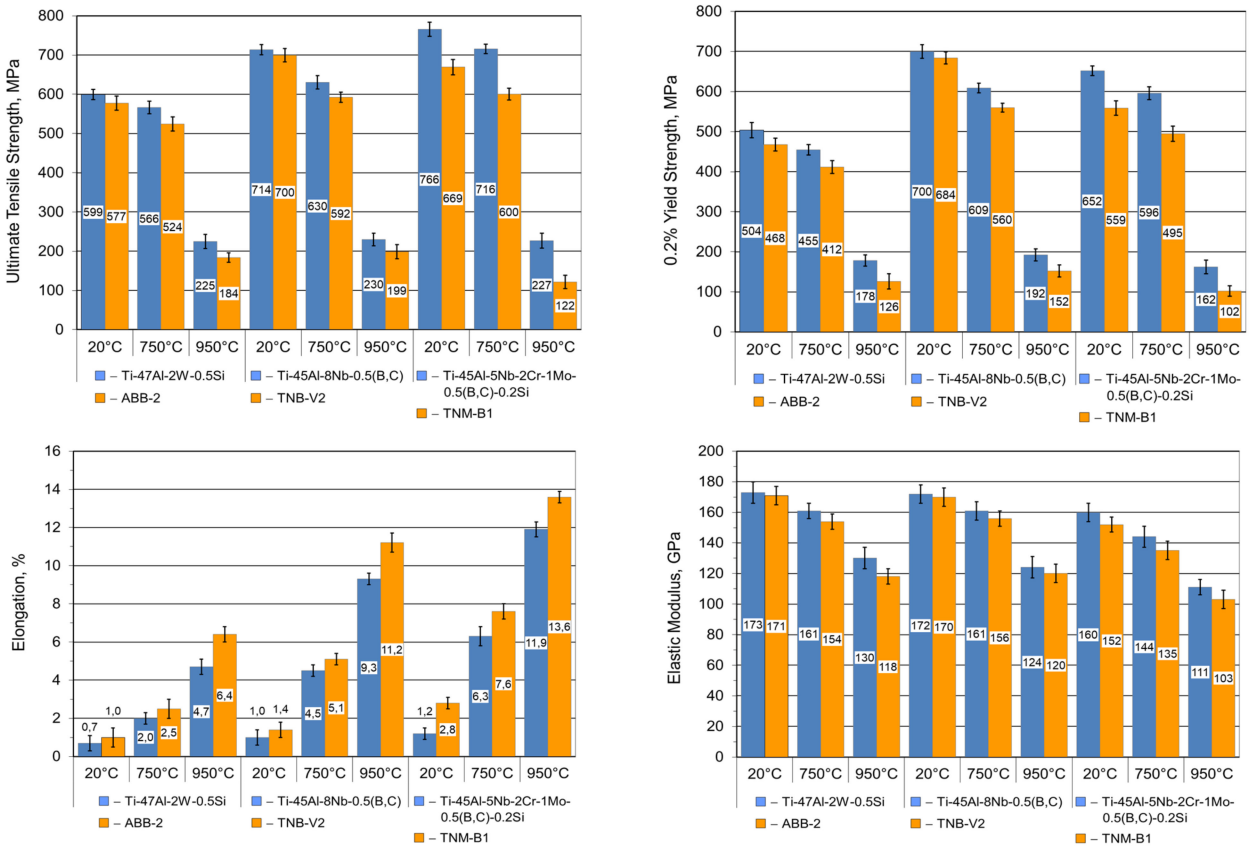

Figure 10. Ultimate tensile strength, 0.2% yield strength, elongation, and Young's modulus of produced and reference alloys at temperature 20, 750, and 950 °C.

Figure 11 shows changes in the strength properties, modulus of longitudinal elasticity, and plastic properties for the produced Ti-45Al-5Nb-2Cr-1Mo-0.5(B,C)-0.2Si alloy, containing the least Al out of all alloys, ~5.0 at.% of Nb, and elements improving the plasticity (Cr) and stabilizing the β phase (Mo), and for the reference TNM-B1 alloy over a wide temperature range from room temperature to 1000 °C. The tensile strength of the Ti-45Al-5Nb-2Cr-1Mo-0.5(B,C)-0.2Si alloy at room temperature is ~770 MPa and the proof stress is approx. 650 MPa. Due to the lowest Al content and the high content of other alloying components as well as silicon, carbon, and boron, which occur as secondary solid solutions and dispersive silicide, carbide, and boride precipitates (Figure 6), the strength properties of this alloy are highest of all the test alloys. These properties remain at a similarly high level at 600 °C, but when the temperature is exceeded, they start decreasing. A particularly significant drop in the strength properties is observed when the temperature exceeds 750 °C. At 1000 °C, the strength properties of the Ti-45Al-5Nb-2Cr-1Mo-0.5(B,C)-0.2Si alloy decrease to the lowest level of all the alloys, which is ~70 and ~50 MPa for the tensile strength and the proof stress, respectively (Figure 11).

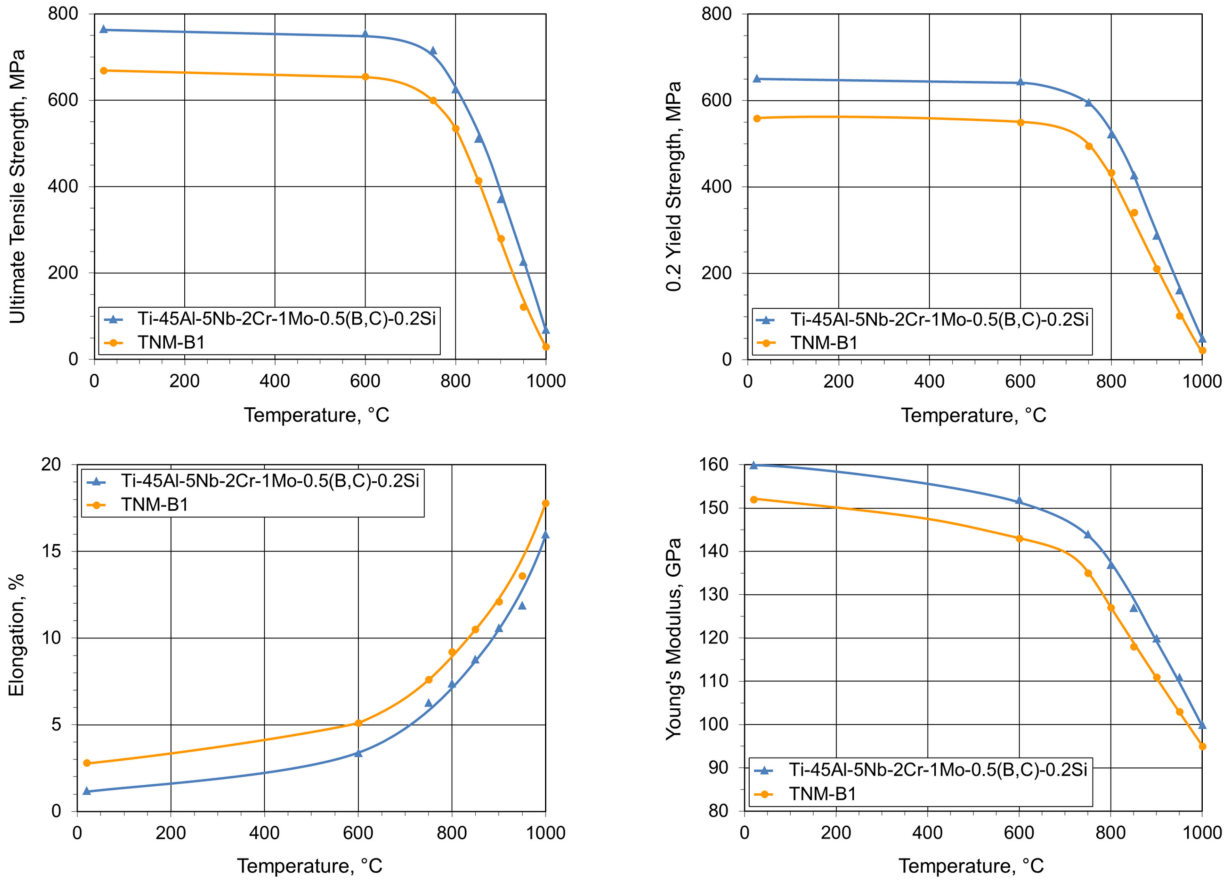

Figure 11. Ultimate tensile strength, 0.2% yield strength, elongation, and Young's modulus of Ti-45Al-5Nb-2Cr-1Mo-0.5(B,C)-0.2Si alloy at temperature between 20 and 1000 °C.

Due to the presence of the ordered β(B2) phase in the phase composition, the Ti-45Al-5Nb-2Cr-1Mo-0.5(B,C)-0.2Si alloy at room temperature has the lowest modulus of longitudinal elasticity of all the alloys, amounting to 160 GPa (Figure 11). The modulus of longitudinal elasticity decreases with the increase in temperature according to the changes in the strength properties, especially when the temperature rises above 750 °C, reaching 100 GPa at 1000 °C.

The changes in the strength properties of the produced Ti-45Al-5Nb-2Cr-1Mo-0.5(B,C)-0.2Si alloy are accompanied by the appropriate changes in the plastic properties in the form of elongation (Figure 11). Due to the presence of the plastic β(B2) phase in the structure of the alloy, its elongation at room temperature reaches the highest level in the group of the test alloys, which is expected for the technological reasons and amounts to 1.2%. The elongation of the alloy clearly increases with increase in temperature, especially after exceeding 600 °C, which is the starting brittle-to-ductile transition temperature for this alloy, reaching ~16.0% at 1000 °C.

The course of changes in the properties of the reference TNB-V2 alloy is very similar to that of the produced Ti-45Al-5Nb-2Cr-1Mo-0.5(B,C)-0.2Si alloy, although its strength properties and modulus of longitudinal elasticity are significantly lower and the plastic properties are higher over the entire temperature range (Figure 11). At room temperature, the tensile strength and proof stress of the reference alloy are lower by ~100 MPa, its modulus of longitudinal elasticity is lower by ~10 GPa, and the elongation is higher by ~1.5% in relation to the produced Ti-45Al-5Nb-2Cr-1Mo-0.5(B,C)-0.2Si alloy. The differences in the properties of the alloys being compared decrease progressively with the increase in temperature, reaching the lowest variation at 1000 °C. The reasons for the higher strength properties and lower plasticity of the produced Ti-45Al-5Nb-2Cr-1Mo-0.5(B,C)-0.2Si alloy

compared to the properties of the reference TNB-V2 alloy should be sought primarily in the varying effectiveness of the solid solution and precipitation hardening due to Nb level which is higher by ~0.7 at.%, Cr level higher by ~1.8 at.%, and Si level higher by ~0.2 at.% and a significantly higher carbon and boron content (by ~0.3 at.% in total) in the produced alloy.

For high-temperature applications, the major concern, apart from the tensile strength and yield strength, is the creep strength, which determines the application range of TiAl-based alloys in competition with other structural materials. The comparative short-term creep tests carried out for the produced and reference alloys under the standard conditions applicable to this group of alloys provided the information on the course of the creep process and allowed the suitability of the alloys for operation at elevated temperature and stress to be determined. They also allowed for the assessment of the effect of carbon on the creep resistance and the course of the creep process. The results of these tests are presented in Figure 12 and Table 4. The creep curves of the produced Ti-47Al-2W-0.5Si alloy (Figure 12) and the remaining alloys generally show the primary creep stage, characterized by a variable, decreasing strain rate, and the secondary creep stage for which the strain rate is constant. There was no accelerated tertiary creep stage for which the strain rate increases until failure. The secondary creep rate of the research alloys was determined over a range of strains from the beginning of the secondary creep stage (the time and creep strain at which the beginning of the secondary creep stage occurs for each alloy are given in Table 4) to the end of the creep test. The Ti-47Al-2W-0.5Si alloy melted in a special graphite crucible and subjected to creep test at 760 °C and 207 MPa reaches the strain of 0.1 and 0.2% at the secondary creep phase after 12 and 49 h, respectively. After 76 h of testing and at the strain of 0.23%, the alloy enters the secondary creep phase, which takes place at 9.8×10^{-6} h^{-1}. At this creep rate, the alloy reaches the strain of 0.5% hypothetically after 355 h, whereas the reference ABB-2 alloy also reaches the strain of 0.1 and 0.2% at the secondary creep phase, after 10 and 38 h, respectively. The reference ABB-2 alloy enters the secondary creep phase at a higher rate of 1.1×10^{-5} h^{-1} after 59 h of testing and at the strain of 0.23%. Under these creep conditions, the reference alloy reaches the strain of 0.5% hypothetically after 324 h.

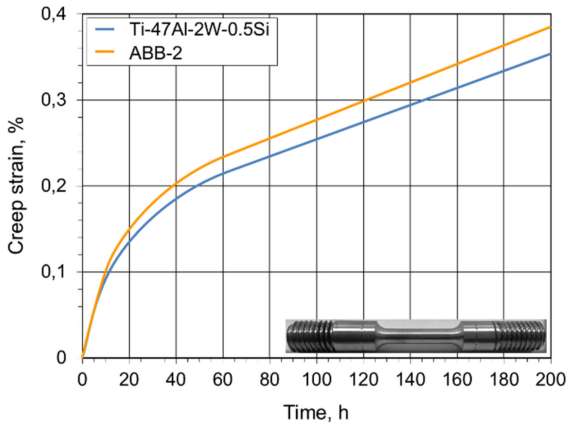

Figure 12. Creep strain vs. time for Ti-47Al-2W-0.5Si alloy tested at 760 °C and 207 MPa.

Other papers of the authors of this study [19] showed the possibility of substantially improving the creep characteristics of the produced Ti-47Al-2W-0.5Si alloy after the application of the special multi-stage heat treatment operations, which refine the grain and increase the lamellar dispersion of the microstructure [41,42]. Following this treatment, the Ti-47Al-2W-0.5Si alloy enters the secondary creep after 70 h at a strain of merely 0.06%. The creep rate of 6.9×10^{-6} h^{-1} or lower makes the alloy to reach the strain of 0.1, 0.2, and 0.5% after 128, 273, and 708 h, respectively. The results of the creep tests carried out on the manufactured Ti-47Al-2W-0.5Si alloy are better than those obtained by Lapin et al. [43,44] and in the US laboratory tests [45]. According to the latter [45], an alloy with a similar

chemical composition reaches the strain of 0.5% at 760 °C and 140 MPa after 650 h. When melted in an induction furnace with a special graphite crucible, the Ti-47Al-2W-0.5Si alloy subjected to the special multi-stage heat treatment [19] reaches the strain of 0.5% after 708 h test at a temperature of 760 °C and stress of 207 MPa, i.e., higher by 50%.

Table 4. Results of creep test of produced and reference alloys.

Alloy	Secondary Creep Condition	Secondary Creep Rate, h^{-1}	Time to Reaches the Strain of, h		
			0.1%	0.2%	0.5%
Ti-47Al-2W-0.5Si	76 h/0.23%	9.8×10^{-6}	12	49	355 *
ABB-2	59 h/0.23%	1.1×10^{-5}	10	38	324 *
Ti-45Al-8Nb-0.5(B,C)	87 h/0.16%	5.3×10^{-6}	26	160	728 *
TNB-V2	100 h/0.22%	6.3×10^{-6}	26	108	544 *
Ti-45Al-5Nb-2Cr-1Mo-0.5(B,C)-0.2Si	70 h/0.56%	1.6×10^{-5}	1	4	20
TNM-B1	74 h/0.57%	1.9×10^{-5}	1	3	14

* determined by approximation based on creep curve

The results of the short-term creep tests for the produced and reference alloys summarized in Table 4 make it possible to conclude that the creep resistance of these alloys under the comparable and standard conditions is similar, however with an advantage on side of all the manufactured alloys. An improved creep resistance of all the produced alloys compared to the reference ones results from the differences in chemical composition of both types of alloys and is likely to be attributed to the higher carbon and boron content in the produced alloys compared to the reference ones (Table 1) and the presence of borides and carbides in the microstructure of the alloy (Figures 5 and 6).

However, in TiAl-based alloys, a pronounced secondary creep stage is often not observed by Schnabel and Scheider [46]. Instead, primary creep is often directly followed by tertiary creep, that is, by an increasing creep rate according to Appel et al. [1]. The presence of the distinct secondary creep stage on the creep curves of the produced alloys with an increased carbon content may be due to the occurrence of dispersive precipitates of carbides, effectively hindering the movement of dislocations and delaying the transition to the accelerated tertiary creep stage.

The short-term creep tests showed limited suitability of the produced Ti-45Al-5Nb-2Cr-1Mo-0.5(B,C)-0.2Si alloy and the reference TNM-B1 alloy for operation under their expected operating conditions due to the excessively high strain during the initial period of the primary creep stage. It seems that it is caused by the presence of the ordered β(B2) phase in the alloy, which has a favorable effect on its formability under hot working conditions and an unfavorable effect on its behavior under creep conditions. A solution to this problem should be sought in minimizing the content of the β(B2) phase in the alloys, e.g., by the application of the special heat treatment processes [47].

The mechanical resistance and creep resistance are considered to be very important for the structural parts. The creep damage is the main failure mode of TiAl-Nb alloys in the high-temperature service. For rotating components like turbine blades, creep resistance of the blade material is of primary importance [48]. The linear thermal expansion coefficients are also extremely important under the conditions of coexistence TiAl-based alloys with titanium and nickel alloys. The lower value of the linear thermal expansion coefficients of the TiAl-based alloys guarantees greater dimensional stability of the elements made of them [38].

4. Conclusions

Three TiAl intermetallic alloys of different generations with a nominal chemical composition—Ti-47Al-2W-0.5Si, Ti-45Al-8Nb-0.5(B,C), and Ti-45Al-5Nb-2Cr-1Mo-0.5(B,C)-0.2Si (at.%)—were successfully melted in an induction furnace with a crucible made of high-density isostatic pressed graphite and gravity cast into graphite molds. The obtained

alloys have the purity equal to that of alloys melted in cold copper crucible furnaces and the carbon content of ~0.35 at.% (0.1 wt.%), which is acceptable for these alloys. The presence of carbon is the result of the graphite crucible degradation due to the effects of reactive liquid titanium and the penetration of the crucible material into molten alloys.

The produced alloys after homogenizing and hot isostatic pressing have lamellar (Ti-47Al-2W-0.5Si), pseudo-lamellar (Ti-45Al-8Nb-0.5(B,C), or duplex (Ti-45Al-5Nb-2Cr-1Mo-0.5(B,C)-0.2Si) microstructure, which consists of the intermetallic γ and α_2 phases, ordered β(B2) phase, carbides, and silicides in the silicon-containing alloys or borides in the boron-containing alloys.

The strength properties of the produced alloys are higher compared to the reference ones. By comparing the results obtained at room and working temperature (750 °C) for the Ti-47Al-2W-0.5Si alloy, we have found that the tensile strength is higher by 22 and 22 MPa, which is 3.8 and 4.19%, respectively; for the Ti-45Al-8Nb-0.5(B,C) alloy, it is higher by 14 and 38 MPa, which is 2 and 6.4%, respectively; while for the Ti-45Al-5Nb-2Cr-1Mo-0.5(B,C)-0.2Si (at.%), it is higher by approximately 97 and 116 MPa, which is 14.0 and 19.3%, respectively.

The produced alloys also have lower ductility compared to the reference ones. Thus, at 20 °C and 750 °C, the elongation for Ti-47Al-2W-0.5Si alloy is lower by 0.3 and 0.5% (30 and 20%, respectively), for the Ti-45Al-8Nb-0.5(B,C) alloy by 0.4 and 0.6% (28.5 and 11.7%, respectively), and for the Ti-45Al-5Nb-2Cr-1Mo-0.5(B,C)-0.2Si (at.%) by 0.6 and 1.3% (21.0 and 17.1%, respectively).

It has been demonstrated that the TiAl intermetallic alloys of different generations produced with the developed technology have similar microstructures and physical, chemical, mechanical, and operating properties at the level comparable to or higher than the properties of the reference alloys with similar chemical compositions melted in the cold copper crucible furnaces.

The observed minor deviations between the properties of the compared alloys produced with the unique technology and the reference alloys are the result of slight differences in their chemical compositions—in particular, the content of aluminum, which is decisive for the proportion of the γ and α_2 phases, and carbon, which determines the efficiency of the solid solution and precipitation hardening mechanisms—rather than the application of different manufacturing processes.

The investigations carried out have shown that the proposed unique and significantly cheaper proprietary technology of melting in induction vacuum furnaces using special crucibles made of high-density isostatic pressed graphite can be successfully used in the production of different generations of TiAl intermetallic alloys.

Author Contributions: Drafting the manuscript, analysis and interpretation of data, and conception and design of study, W.S.; sample preparation, microstructure research and analysis, and analysis of mechanical and physical properties date, A.S. All authors have read and agreed to the published version of the manuscript.

Funding: Silesian University of Technology (Faculty of Materials Engineering)—Poland, supported this work as a part of Statutory Research fund number 11/030/BK_20/0285.

Data Availability Statement: All the data generated during this study are included in this article.

Conflicts of Interest: The authors declare no conflict of interest.

References

1. Appel, F.; Paul, J.D.H.; Oehring, M. *Gamma Titanium Aluminide Alloys-Science and Technology*; John Wiley & Sons: Hoboken, NJ, USA, 2011.
2. Bewlay, B.P.; Nag, S.; Suzuki, A.; Weimer, M.J. TiAl alloys in commercial aircraft engines. *Mater. High. Temp.* **2016**, *33*, 549–559. [CrossRef]
3. Clemens, H.; Mayer, S. Advanced Intermetallic TiAl Alloys. *Mater. Sci. Forum* **2016**, *879*, 113–118. [CrossRef]
4. Kim, Y.W.; Kim, S.L. Advances in Gammalloy Materials-Processes-Application Technology: Successes, Dilemmas, and Future. *JOM* **2018**, *70*, 553–560. [CrossRef]

5. Burtscher, M.; Klein, Y.; Lindemann, J.; Lehmann, O.; Fellmann, H.; Güther, V.; Clemens, H.; Mayer, S. An Advanced TiAl Alloy for High-Performance Racing Applications. *Materials* **2020**, *13*, 4720. [CrossRef]
6. Wimler, D.; Lindemann, J.; Reith, M.; Kirchner, A.; Allen, M.; Vargas, W.G.; Franke, M.; Kloden, B.; Weißgarber, T.; Güther, V.; et al. Designing advanced intermetallic titanium aluminide alloys for additive manufacturing. *Intermetallics* **2021**, *131*, 1–10. [CrossRef]
7. Mogale, N.F.; Matizamhuka, W.R. Spark Plasma Sintering of Titanium Aluminides: A Progress Review on Processing, Structure-Property Relations, Alloy Development and Challenges. *Metals* **2020**, *10*, 1080. [CrossRef]
8. Kamyshnykova, K.; Lapin, J. Induction melting and centrifugal casting of intermetallic TiAl alloy. In Proceedings of the International Conference "Mechanical Technologies and Structural Materials", Split, Croatia, 22–23 September 2016.
9. Fashu, S.; Lototskyy, M.; Davids, M.W.; Pickering, L.; Linkov, V.; Tai, S.; Renheng, T.; Fangming, X.; Fursikov, P.V.; Tarasov, B.P. A review on crucibles for induction melting of titanium alloys. *Mater. Des.* **2020**, *186*, 1–17. [CrossRef]
10. Barbosa, J.; Ribeiro, C.S. Influence of crucible material on the level of contamination in TiAl using induction melting. *Int. J. Cast Met. Res.* **2000**, *12*, 293–301. [CrossRef]
11. Kostov, A.; Friedrich, B. Selection of crucible oxides in molten titanium and titanium aluminium alloys by thermo-chemistry calculations. *J. Min. Metall.* **2005**, *41*, 113–125. [CrossRef]
12. Barbosa, J.; Ribeiro, C.S.; Monteiro, C. The Production of TiAl by Foundry Processes. *Key Eng. Mater.* **2002**, *230–232*, 106–109. [CrossRef]
13. Čegan, T.; Szurman, I.; Kursa, M. Preparation of TiAl based alloys by induction melting in graphite crucibles. *Kov. Mater.* **2015**, *53*, 69–78.
14. Čegan, T.; Cagala, M.; Kursa, M.; Kawulok, P.; Rusz, S.; Jurica, J.; Vontorová, J. Effect of Ti_2AlC particles on the microstructure and elevated-temperature-deformation properties of γ-TiAl alloys. *Mater. Technol.* **2014**, *48*, 831–835.
15. Kamyshnykova, K.; Lapin, J. Vacuum induction melting and solidification of TiAl-based alloy in graphite crucibles. *Vacuum* **2018**, *154*, 218–226. [CrossRef]
16. Klimová, A.; Lapin, J.; Pelachová, T. Characterization of TiAl based alloys with various content of carbon. *IOP Conf. Ser. Mater. Sci. Eng.* **2017**, *179*, 12038. [CrossRef]
17. Lapin, J.; Kamyshnykova, K.; Klimova, A. Comparative Study of Microstructure and Mechanical Properties of Two TiAl-Based Alloys Reinforced with Carbide Particles. *Molecules* **2020**, *25*, 3423. [CrossRef]
18. Li, M.; Xiao, S.; Xiao, L.; Xu, L.; Tian, J.; Chen, Y. Effects of carbon and boron addition on microstructure and mechanical properties of TiAl alloys. *J. Alloy. Compd.* **2017**, *728*, 206–221. [CrossRef]
19. Szkliniarz, A.; Szkliniarz, W. Microstructure and Properties of Ti-47Al-2W-0.5Si Cast Alloy. *Solid State Phenom.* **2015**, *226*, 3–6. [CrossRef]
20. Szkliniarz, A.; Szkliniarz, W. Microstructure and Properties of a New Generation of TiAl Based Alloys. *Solid State Phenom.* **2015**, *229*, 125–130. [CrossRef]
21. Szkliniarz, W.; Szkliniarz, A. Fundamentals of manufacturing technologies for aircraft engine parts made of TiAl based alloys. *Arch. Metall. Mater.* **2016**, *61*, 1385–1390. [CrossRef]
22. Szkliniarz, W.; Szkliniarz, A. The characteristics of TiAl-based alloys melted in graphite crucibles. *Mater. Sci. Technol.* **2019**, *35*, 297–305. [CrossRef]
23. Szkliniarz, W.; Szkliniarz, A. The Chemical Composition and Microstructure of Ti-47Al-2W-0.5Si Alloy Melted in Ceramic Crucibles. *Solid State Phenom.* **2012**, *191*, 211–220. [CrossRef]
24. Barbosa, J.; Ribeiro, C.S.; Monteiro, C. Processing of γTiAl, by ceramic crucible induction melting, and pouring in ceramic shells. *Mater. Sci. Forum* **2003**, *426–432*, 1933–1938. [CrossRef]
25. Čegan, T.; Szurman, I. Thermal stability and precipitation strengthening of fully lamellar Ti-45Al-5Nb-0.2B-0.75C alloy. *Met. Mater.* **2018**, *55*, 421–430.
26. Stark, A.; Oehring, M.; Pyczak, F.; Schell, N. Carbon in Nb-Rich γ-TiAl Based Alloys. Available online: https://photon-science.desy.de/annual_report/files/2010/20101235.pdf (accessed on 7 March 2021).
27. Scheu, C.; Stergar, E.; Schaber, M. High carbon solubility in a γ-TiAl based Ti-45Al-5Nb-0.5C alloy and its effect on hardening. *Acta Matter.* **2009**, *57*, 1504–1511. [CrossRef]
28. Schwaighofer, E.; Rashkova, B.; Clemens, H.; Stark, A.; Mayer, S. Effect of carbon addition on solidification behavior, phase evolution and creep properties of an intermetallic β-stabilized γ-TiAl based alloy. *Intermetallics* **2014**, *46*, 173–184. [CrossRef]
29. Klein, T.; Clemens, H.; Mayer, S. Advancement of Compositional and Microstructural Design of Intermetallic γ-TiAl Based Alloys Determined by Atom Probe Tomography. *Materials* **2016**, *9*, 755. [CrossRef]
30. Kawabata, T.; Tadano, M.; Izumi, O. Effect of Carbon and Nitrogen on Mechanical Properties of TiAl Alloys. *ISIJ Int.* **1991**, *31*, 1161–1167. [CrossRef]
31. Kim, Y.W.; Kim, S.L. Effects of microstructure and C and Si additions on elevated temperature creep and fatigue of gamma TiAl alloys. *Intermetallics* **2014**, *53*, 92–101. [CrossRef]
32. Klein, T.; Schachermayer, M.; Mendez-Martin, F.; Schöberl, T.; Rashkova, B.; Clemens, H.; Mayer, S. Carbon distribution in multi-phase γ-TiAl based alloys and its influence on mechanical properties and phase formation. *Acta Mater.* **2015**, *94*, 205–213. [CrossRef]
33. Yun, J.H.; Oh, M.H.; Nam, S.W.; Wee, D.M.; Inui, H.; Yamaguchi, M. Microalloying Effects in TiAl + Mo Alloys. *Mater. Sci. Eng. A* **1997**, *239–240*, 702–708. [CrossRef]

34. Gerling, R.; Schimansky, F.P.; Stark, A.; Bartels, A.; Kestler, H.; Chad, L.; Scheud, C.; Clemens, H. Microstructure and mechanical properties of Ti 45Al 5Nb+(0-0.5C) sheets. *Intermetallics* **2008**, *16*, 689–697. [CrossRef]
35. Chu, Y.; Li, J.; Zhu, L.; Liu, Y.; Tang, B.; Kou, H. Microstructure Evolution of a High Nb Containing TiAl Alloy with ($\alpha 2 + \gamma$) Microstructure during Elevated Temperature Deformation. *Metals* **2018**, *8*, 916. [CrossRef]
36. Hu, D. Role of boron in TiAl alloy development: A review. *Rare Met.* **2016**, *35*, 1–14. [CrossRef]
37. Li, M.; Xiao, S.; Chen, Y.; Xu, L.; Tian, J. The effect of boron addition on the high-temperature properties and microstructure evolution of high Nb containing TiAl alloys. *Mater. Sci. Eng. A* **2018**, *733*, 190–198. [CrossRef]
38. Staron, P.; Stark, A.; Schell, N.; Spoerk-Erdely, P.; Clemens, H. Thermal Expansion of a Multiphase Intermetallic Ti-Al-Nb-Mo Alloy Studied by High-Energy X-ray Diffraction. *Materials* **2021**, *14*, 727. [CrossRef]
39. Leyens, C.; Peters, M. *Titanium and Titanium Alloys*; John Wiley & Sons: Hoboken, NJ, USA, 2003.
40. Szkliniarz, A.; Moskal, G.; Szkliniarz, W.; Swadźba, R. Improvement of oxidation resistance of Ti-47Al-2W-0.5Si alloy modified by aluminizing method. *Surf. Coat. Technol.* **2015**, *277*, 270–277. [CrossRef]
41. Kościelna, A.; Szkliniarz, W. Effect of cyclic heat treatment parameters on the grain refinement of Ti-48Al-2Cr-2Nb alloy. *Mater. Charact.* **2009**, *60*, 1158–1162. [CrossRef]
42. Szkliniarz, A.; Szkliniarz, W. Multi-Stage Heat Treatment of Second Generation TiAl Based Alloys. *Solid State Phenom.* **2013**, *211*, 129–140. [CrossRef]
43. Lapin, J.; Nazmy, M. Microstructure and creep properties of a cast intermetallic Ti-46Al-2W-0.5Si alloy for gas turbine applications. *Mater. Sci. Eng. A* **2004**, *380*, 298–307. [CrossRef]
44. Lapin, J. Creep behaviour of a cast TiAl-based alloy for industrial applications. *Intermetallics* **2006**, *14*, 115–122. [CrossRef]
45. Deevi, S.C.; Zhang, W.J. Creep Resistant Titanium Aluminide Alloys. U.S. Patent US 6,425,964 B1, 30 July 2002.
46. Schnabel, J.E.; Scheider, I. Crystal Plasticity Modeling of Creep in Alloys with Lamellar Microstructures at the Example of Fully Lamellar TiAl. *Front. Mater.* **2021**, *7*, 581187. [CrossRef]
47. Kastenhuber, M.; Rashkova, B.; Clemens, H.; Mayer, S. Enhancement of creep properties and microstructural stability of intermetallic β-solidifying γ-TiAl based alloys. *Intermetallics* **2015**, *63*, 19–26. [CrossRef]
48. Zhang, S.; Tian, S.; Lv, X.; Yu, H.; Tian, N.; Jiao, Z.; Zhao, G.; Li, D. Deformation and damage behaviors of as-cast TiAl-Nb alloy during creep. *Prog. Nat. Sci. Mater. Int.* **2018**, *28*, 618–625. [CrossRef]